Electronic structures of three semiconducting intermetallics: $RuAl_2$, $RuGa_2$, and $OsAl_2$

1998 J. Phys.: Condens. Matter 10 701

(http://iopscience.iop.org/0953-8984/10/3/021)

J. Phys.: Condens. Matter **10** (1998) 701–716. Printed in the UK PII: S0953-8984(98)86154-7

Electronic structures of three semiconducting intermetallics: $RuAl_2$, $RuGa_2$, and $OsAl_2$

Michael Springborg† and Rüdiger Fischer‡

† Department of Chemistry, University of Konstanz, D-78457 Konstanz, Germany
‡ Department of Physics, University of Konstanz, D-78457 Konstanz, Germany

Received 15 July 1997, in final form 8 September 1997

Abstract. Results of first-principles, density-functional, LMTO-ASA calculations on the closely related C11, C40, and C54 structures of the three title compounds are reported. Only for $OsAl_2$ in the C11 structure were the structural degrees of freedom optimized; this gave results in good agreement with experimental values. On the other hand, the calculations were not capable of reproducing the correct relative stability of the different structures; this was ascribed to the atomic-sphere approximation. All of the compounds were found to be small-gap semiconductors with, however, a slightly larger gap for $OsAl_2$. The occurrence of a gap at the Fermi level is mainly due to hybridization between d functions of Os or Ru and p functions of Al or Ga, but, in particular for $OsAl_2$, charge-transfer effects can also be considered to be responsible for the occurrence of a gap. Several flat bands just above the Fermi level lead to a corresponding high density of states there, but also to low carrier velocities. As a by-product we propose a scheme for studying current densities using parameter-free methods, and by applying this approach to the title compounds we predict that they will prove to have transport properties similar to those of Si, and that in particular the n-doped systems should be interesting from a technological point of view.

1. Introduction

The possibility of selecting materials with specific properties for special purposes is currently as important as ever. For semiconductors, the field is dominated by silicon, which for most purposes satisfies the requirements of the applications. However, when one is attempting to modify optical or transport properties, the possibilities of silicon are limited, and one has to look for alternative materials. Here, intermetallic compounds offer an interesting alternative. First of all, one may hope that these materials will form ideal interfaces with conventional metals, and hence that it will be found that systems based on these materials can easily be integrated into various devices. Moreover, one may speculate that their properties will prove to lie in between those of metals and more traditional semiconductors, and most notably that they will be found to have small band gaps and excellent transport properties. Finally, it is, from the point of view of basic science, interesting to understand how the semiconducting properties are derived from those of the metallic constituents.

The title compounds of this work are such materials. $RuAl_2$ crystallizes in the $TiSi_2$ structure [1, 2], also called the C54 structure. The chemical formula gives mole fractions of 67% Al atoms and 33% transition-metal atoms, which are very close to those observed for the Al-based quasicrystals. There have consequently been several studies devoted to comparing this material with the quasicrystals (see, e.g., [3–9]) whereas studies devoted to its semiconducting properties are scarce. $OsAl_2$, on the other hand, crystallizes in the

0953-8984/98/030701+16$19.50

$MoSi_2$ structure [10], also called the C11 structure. Despite the similarity with $RuAl_2$ (see below), it has not been the subject of any studies of electronic properties. Finally, $RuGa_2$ crystallizes in the C54 structure [11–13]. Only one study has been devoted to the electronic structure of this compound [3], and as for $RuAl_2$ only the C54 structure was considered.

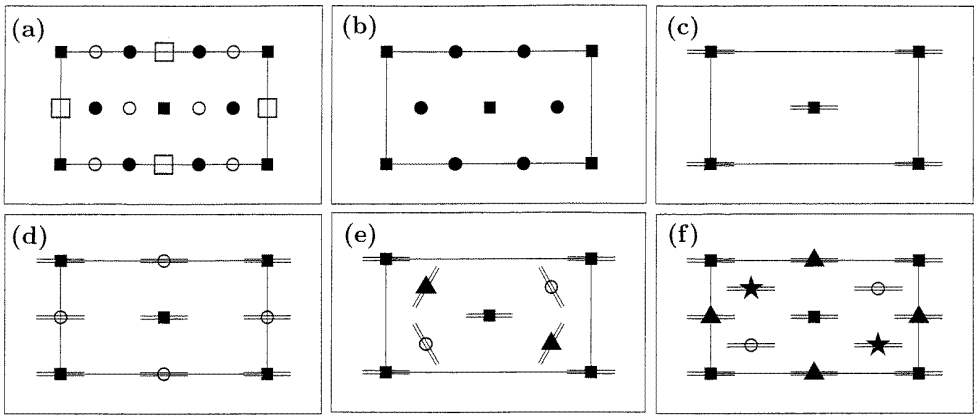

Figure 1. A schematic representation of the different crystal structures using the common monoclinic structure. Each subfigure shows the positions of the atoms projected onto the (x, y)-plane. (a) shows the C11 structure with the squares representing the Ru or Os atoms, and the circles representing the Al or Ga atoms. The atoms represented with filled symbols are all lying in one layer, and those represented with open symbols lie in the next one on top of the first one. (b) shows one such layer and (c) shows a simple representation of (b). Here, only the Ru or Os atoms are shown, whereas the bonds to the Al or Ga atoms of the same layer are shown as double lines. The complete C11 structure is then shown in (d) with the Ru or Os atoms of the same layer represented by the same symbol. (e) shows the equivalent representation for the C40 structure and (f) that of the C54 structure. Here, the order of the layer stacking is filled square, followed by open circle, followed by filled triangle, and, for the C40 structure, followed by star. The basis vectors $\boldsymbol{a}'$ and $\boldsymbol{b}'$ of table 4 (see later) are along the x-axis and y-axis, respectively, whereas the $\boldsymbol{c}'$-axis is approximately perpendicular to the planes. In the electron-density contour maps we have placed the origin at the midpoint of the lower side.

The $TiSi_2$ (C54), the $MoSi_2$ (C11), and the $CrSi_2$ (C40) structures are closely related, as shown in figure 1. All three structures may be described within an orthorhombic supercell, and as consisting of stacked planes containing linear MX_2 units. For the C54 and the C11 structures these planes are all parallel, whereas for the C40 structure they are rotated with respect to each other. For the C11, C40, and C54 structures the stacking repeats itself after two, three, and four planes, respectively, along the stacking direction. For all of the structures the M atoms are each surrounded by ten X atoms, whereas the X atoms have five X atoms and five M atoms as nearest neighbours. It is obvious from the discussion above that the C54 structure is the most relevant one for the present compounds. This structure has been known of since the end of the 1930s [14, 15]. But the other two structures are closely related to this one, and it is therefore interesting to compare all three.

It is noteworthy that $OsAl_2$ crystallizes in the C11 structure whereas $RuAl_2$ and $RuGa_2$ crystallize in the C54 structure, although Os and Ru are very similar, as are Al and Ga. In addition, $OsGa_2$ is only stable at high pressure (and crystallizes then in the C54 structure), whereas at standard pressure it possesses a miscibility gap, and separates into OsGa and $OsGa_3$. Thus, it can be expected that the quasibinary $Ru_xOs_{1-x}Al_2$ and quasiternary $Ru_xOs_{1-x}Al_yGa_{2-y}$ systems will also prove to possess miscibility gaps, and that different

phases will be found to have different crystal structures.

Such behaviour has been observed by Nowotny *et al* [16–18] for $Ti_xMo_{1-x}Si_2$, $MnAl_{2-x}Si_x$, and $MoAl_{2-x}Si_x$ systems, for which phases with C11, C40, and C54 structures were identified. In these cases, however, the relative stability of the different structures was ascribed to different valence-electron concentrations (VEC). For the systems of the present work, Ru and Os (as well as Ga and Al) have the same valency, so it is not likely that variations in the VEC are responsible for the occurrence of the different phases. But the results of Nowotny *et al* [16–18], as well as the similarity of the three crystal structures of figure 1, suggest that a complete study of the pure $RuAl_2$, $RuGa_2$, and $OsAl_2$ systems should include all three crystal structures.

In order to obtain detailed information on the electronic properties of the pure phases of $RuAl_2$, $RuGa_2$, and $OsAl_2$, and how they are influenced by the structure, we have therefore studied all three crystallographic structures for all three compounds by means of first-principles density-functional calculations. We have applied the LMTO-ASA method [19], which will be briefly described in section 2. In this section we shall also propose a system for studying current densities using parameter-free methods. Except for one case, we have not made any attempt to optimize the structural parameters, but have considered either experimental ones, when available, or realistic ones (see section 2). Section 3 contains the results, and we give our conclusions in section 4.

2. The computational method

We apply the LMTO-ASA method of Andersen [19]. This method is based on the density-functional formalism of Hohenberg and Kohn [20] in the formulation of Kohn and Sham [21]. The solutions to the Kohn–Sham equations are expanded in terms of a set of linearized muffin-tin orbitals (LMTOs). In our calculations we used a set consisting of one set of s, p, and d functions at each site. Furthermore, the errors due to the ASA (atomic-sphere approximation) are removed perturbatively through the so-called combined-correction terms [19].

In the present calculations we described the Ne core of the Al atoms, the Cu core of the Ga atoms, the Kr core of the Ru atoms, and the Yb core of the Os atoms within a frozen-core approximation. Moreover, for each compound and structure all sphere radii were treated as being identical.

The systems of interest here are crystalline, and the eigenfunctions ψ_i become Bloch waves characterized by a Bloch vector $\boldsymbol{k}$. The corresponding $\boldsymbol{k}$-space samplings, like, e.g., that in equation (3), are performed using the tetrahedron method [22, 23]. For reasons to be made clear below, we shall now briefly describe this method.

The $\boldsymbol{k}$-space is discretized into a set of equidistant points:

$$\boldsymbol{k} = n_x\boldsymbol{k}_a + n_y\boldsymbol{k}_b + n_z\boldsymbol{k}_c. \tag{1}$$

$|\boldsymbol{k}_a|$, $|\boldsymbol{k}_b|$, and $|\boldsymbol{k}_c|$ may, but need not, be identical. The Kohn–Sham equations are only solved for this discrete set of $\boldsymbol{k}$-points, and, accordingly, only at these points are the eigenvalues ϵ_i known. In order to arrive at information for these $\boldsymbol{k}$-points that is not included above, one introduces microcells (rectangular boxes in $\boldsymbol{k}$-space) constructed from the eight $\boldsymbol{k}$-points defined by n_i and $n_i + 1$ ($i = x, y, z$). Subsequently, each of these boxes is split into six tetrahedra, of which the corners are defined by four of the eight $\boldsymbol{k}$-points, and which furthermore fulfil the requirement that none cuts the boundaries of the first Brillouin zone. From the energy eigenvalues at the corners of such a tetrahedron, one finally performs a linear interpolation for the energy values at any $\boldsymbol{k}$-point inside the tetrahedron.

We will be particularly interested in the optical and transport properties of these materials. For the former, the band structures as well as the densities of states provide the relevant information and there is no need for rearrangement. For the latter, we study the electrical and thermal current densities. These can be obtained from the current-density matrices (see, e.g., [24]):

$$\mathbf{L}^{\alpha} = -\frac{e^2}{4\pi^3}\int \frac{\partial f}{\partial \epsilon}\tau[\epsilon(\boldsymbol{k})]\boldsymbol{v}(\boldsymbol{k})\boldsymbol{v}(\boldsymbol{k})[\epsilon(\boldsymbol{k})-\epsilon_F]^{\alpha}\ \mathrm{d}\boldsymbol{k}. \tag{2}$$

Here, $f(\epsilon, T, \epsilon_F)$ is the Fermi–Dirac distribution, ϵ_F is the Fermi energy, and $\tau(\epsilon)$ is the carrier mean lifetime. Finally, the semi-classical carrier velocity is given by

$$\boldsymbol{v}(\boldsymbol{k}) = \frac{1}{\hbar}\boldsymbol{\nabla}_{\boldsymbol{k}}\epsilon(\boldsymbol{k}). \tag{3}$$

Due to the inclusion of the factor $\partial f/\partial\epsilon$, the major contributions to the integrals in equation (2) come from a narrow interval of width roughly kT around the Fermi energy ϵ_F. By assuming that $\tau[\epsilon(\boldsymbol{k})]$ is independent of $\boldsymbol{k}$ and introducing the partial conductivity matrix

$$\boldsymbol{\sigma}(\epsilon) = \frac{e^2}{4\pi^3}\tau(\epsilon)\int \boldsymbol{v}(\boldsymbol{k})\boldsymbol{v}(\boldsymbol{k})\delta[\epsilon-\epsilon(\boldsymbol{k})]\ \mathrm{d}\boldsymbol{k} \tag{4}$$

we have

$$\mathbf{L}^{\alpha} = -\int \frac{\partial f}{\partial \epsilon}(\epsilon-\epsilon_F)^{\alpha}\boldsymbol{\sigma}(\epsilon)\ \mathrm{d}\epsilon. \tag{5}$$

The electrical and thermal current densities can be extracted from the current-density matrices for $\alpha = 0$, 1, and 2. Therefore, by analysing

$$\tilde{\boldsymbol{\sigma}}(\epsilon) = \boldsymbol{\sigma}(\epsilon)/\tau(\epsilon) \tag{6}$$

the main features of the transport properties can be studied without having to specify a temperature T and while assuming that τ is (roughly) energy independent. In our work we shall therefore study the transport properties by considering the various components of $\tilde{\boldsymbol{\sigma}}(\epsilon)$.

The calculation of the (i, j) component of $\tilde{\boldsymbol{\sigma}}(\epsilon)$ is very similar to the calculation of the density of states except for the extra factor $v_i(\boldsymbol{k})v_j(\boldsymbol{k})$. Thus, we proceed exactly as described above for the density of states by using the tetrahedron method, but will in addition have to include these factors. For each point $\boldsymbol{k} = \boldsymbol{k}_0$ given by equation (1), the calculations provide the band energies ϵ. Using these as well as those of the eight neighbouring $\boldsymbol{k}$-points (obtained by changing at least one of the n_x, n_y, n_z by ± 1) we assume a linear $\boldsymbol{k}$-dependence (equivalent to the strategy behind the tetrahedron method), i.e.

$$\epsilon(\boldsymbol{k}) = \epsilon(\boldsymbol{k}_0) + \boldsymbol{A}\cdot(\boldsymbol{k}-\boldsymbol{k}_0). \tag{7}$$

The coefficients of $\boldsymbol{A}$ are obtained from a least-squares fit:

$$\frac{\partial}{\partial A_n}\sum_{i=0}^{8}\left[\epsilon(\boldsymbol{k}_i) - \boldsymbol{A}\cdot(\boldsymbol{k}_i-\boldsymbol{k}_0)\right]^2 = 0 \qquad n = 1, 2, 3. \tag{8}$$

The problem of solving equation (8) can be rewritten as that of solving a 3×3 set of linear equations:

$$\mathbf{B}\boldsymbol{A} = \boldsymbol{C} \tag{9}$$

where $\mathbf{B}$ (as well as its inverse) only depends on $(\boldsymbol{k}_a, \boldsymbol{k}_b, \boldsymbol{k}_c)$ in equation (1) and hence need only be calculated once, whereas $\boldsymbol{C}$ depends on the $\boldsymbol{k}$-point $\boldsymbol{k}_0$ through the $\boldsymbol{k}$-dependence

of the band energies. $\boldsymbol{A}$ is essentially the carrier velocity sought, except for prefactors depending on $(\boldsymbol{k}_a, \boldsymbol{k}_b, \boldsymbol{k}_c)$.

Depending on the point-group symmetry of the first Brillouin zone, various off-diagonal elements of the $\tilde{\boldsymbol{\sigma}}(\epsilon)$ matrix may vanish independently of ϵ. We have not, however, made any use of this. Deviations from zero are therefore estimates of the accuracy of these calculations. These deviations have a number of different origins. First of all, as described above, the $\boldsymbol{k}$-space is divided into microcells given by equation (1). These cells will be equivalent for the symmetry operations that may lead to vanishing elements of $\tilde{\boldsymbol{\sigma}}$. For example, any two microcells related through a mirror operation or an inversion will both exist. However, the tetrahedra that are obtained by subdividing the microcells may not be equivalent. One may force them to be, but we have not done so here. Furthermore, in the energy and $\boldsymbol{k}$-space regions where many bands occur, band crossings or avoided crossings may cause additional deviations. This problem has not been explicitly studied here either. Instead we will show our 'rough' results obtained by also using a fairly dense set of $\boldsymbol{k}$-points for the components that should vanish, whereby estimates of the inaccuracies can be obtained.

Table 1. The basis vectors of the three structures considered in this work. For each structure, the vectors are given in units of a lattice constant a that may differ for the different structures as well as for different compounds.

Structure	Basis vectors		
C11	$(1, 0, 0)$	$(0, 1, 0)$	$(-1/2, -1/2, c/a)$
C40	$(1/2, -\sqrt{3}/2, 0)$	$(1/2, \sqrt{3}/2, 0)$	$(0, 0, c/a)$
C54	$(b/a, 0, 0)$	$(-b/2a, 1/2, 0)$	$(b/2a, 0, c/2a)$

Table 2. Positions of the atoms inside the unit cell for the three different structures in units of the basis vectors of table 1. The ideal value for the internal parameter u is $1/3$ for the C11 and the C54 structures, and $1/6$ for the C40 structure. M denotes Ru or Os, whereas X denotes Al or Ga.

Structure	Atom	Positions		
C11	M	$(0, 0, 0)$		
	X	$(u, u, 2u)$	$(\bar{u}, \bar{u}, 2\bar{u})$	
C40	M	$(1/2, 0, 0)$	$(0, 1/2, 2/3)$	$(1/2, 1/2, 1/3)$
	X	$(u/2 + 1/4, \bar{u}/2 + 1/4, 0)$	$(\bar{u}/2 + 1/4, u/2 + 1/4, 2/3)$	$(u, \bar{u}, 1/3)$
		$(\bar{u}/2 - 1/4, u/2 - 1/4, 0)$	$(u/2 - 1/4, \bar{u}/2 - 1/4, 2/3)$	$(\bar{u}, u, 1/3)$
C54	M	$(0, 0, 0)$	$(1/2, 1/4, 1/2)$	
	X	$(2u, u, 0)$	$(2\bar{u} + 1/2, \bar{u} + 1/4, 1/2)$	$(2\bar{u}, \bar{u}, 0)$
		$(2u + 1/2, u + 1/4, 1/2)$		

The basis vectors of the three structures are given in table 1, and in table 2 we give the internal coordinates for the atoms in units of the basis vectors of table 1. Here we notice that the transition-metal atoms (Ru or Os; denoted as M in the table) are located at high-symmetry positions, but that the positions of the Ga or Al atoms are characterized by a parameter u. The ideal value of this is $\frac{1}{3}$ for the C11 and C54 structures but $\frac{1}{6}$ for the C40 structure. In table 3 we list the values that we have used for the structures, as well as those that we have optimized for the $OsAl_2$ compound in the C11 structure. The structural coordinates of $RuGa_2$ and $RuAl_2$ in the C54 structure and of $OsAl_2$ in the C11 structure were chosen very close

Table 3. The parameters defining the different structures of the three compounds according to tables 1 and 2. a is given in atomic units, whereas the other parameters are dimensionless. For $OsAl_2$ in the C11 structure the values in the parentheses are the optimized ones.

Compound	Structure	a (au)	c/a	u	b/a
$RuAl_2$	C11	5.991	1.306	0.335	
$RuAl_2$	C40	8.806	1.423	0.167	
$RuAl_2$	C54	15.141	1.096	0.333	0.589
$RuGa_2$	C11	6.028	1.3025	0.34	
$RuGa_2$	C40	8.882	1.415	0.167	
$RuGa_2$	C54	15.457	1.064	0.333	0.581
$OsAl_2$	C11	5.975 (6.07)	1.313 (1.273)	0.333 (0.341)	
$OsAl_2$	C40	8.806	1.429	0.167	
$OsAl_2$	C54	15.250	1.094	0.333	0.584

Table 4. The smallest interatomic distances (in au) for the different compounds and structures. M denotes Ru or Os, and X is Al or Ga. The 'in-plane' distances are the shortest ones in the planes of figure 1. For the C11 structure the shortest M–X and X–X distances in directions out of these planes are identical to those within the planes.

Compound	Structure	M–M	M–X	M–X (in plane)	X–X	X–X (in plane)
$RuAl_2$	C11	5.99	4.97	4.97	4.98	4.98
$RuAl_2$	C40	6.07	4.89	5.08	4.89	5.08
$RuAl_2$	C54	6.04	4.88	5.05	4.88	5.05
$RuGa_2$	C11	6.03	5.00	5.00	5.00	5.00
$RuGa_2$	C40	6.11	4.91	5.13	4.91	5.13
$RuGa_2$	C54	6.08	4.86	5.16	4.86	5.16
$OsAl_2$	C11	5.97	4.97	4.97	4.97	4.97
$OsAl_2$	C40	6.08	4.91	5.08	4.91	5.08
$OsAl_2$	C54	6.08	4.90	5.08	4.90	5.08

to those observed experimentally for these three compounds [1, 10, 11, 15]. For the other hypothetical structures we have constructed coordinates that lead to very similar nearest-neighbour distances, as demonstrated in table 4, and resembling those available for the other compounds and/or structures. We have thereby used the experimental information of Nowotny *et al* [16–18] on the $Ti_xMo_{1-x}Si_2$, $MnAl_{2-x}Si_x$, and $MoAl_{2-x}Si_x$ mixed systems. They found that the ratios of the distances between the layers of figure 1 for the C11, C40, and C54 structures were 1.08:1.05:1.00. We have used these ratios, and furthermore assumed that for a given compound the three crystal structures have the same density.

The fact that the three compounds have very similar structural parameters can be understood on the basis of the fact that the covalent radii of octahedrally coordinated Ru and Os atoms are essentially identical (2.51 au) as are those of tetrahedrally coordinated Al and Ga atoms (2.38 au) [25]. These radii do in addition lead to bond lengths close to those reported in table 4. We have hereby ignored the fact that the coordinations in the present systems are somewhat different from octahedral and tetrahedral.

With the structural characterization of table 1 we end up with the first Brillouin zones shown in figure 2.

As mentioned in the introduction, it is possible to describe all three structures, C11, C40, and C54, as belonging to the class of centred monoclinic structures. In that case each unit cell contains six formula units. Denoting the basis vectors of the monoclinic structure

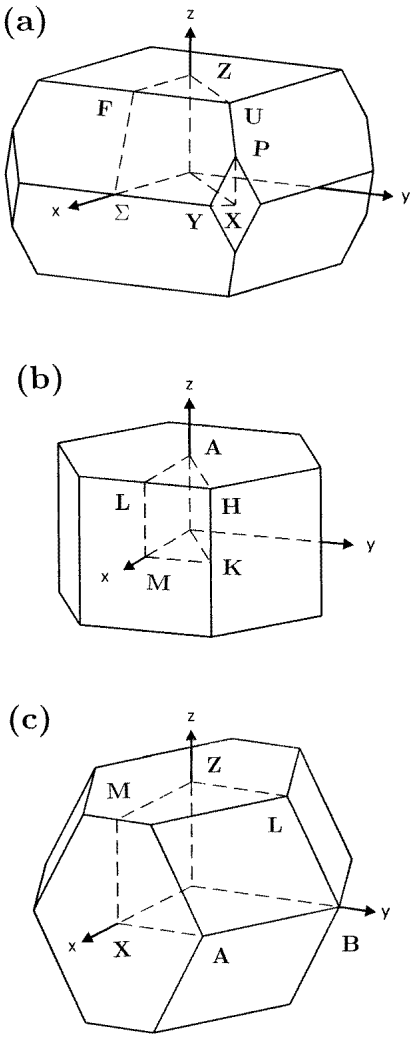

Figure 2. The first Brillouin zone of the (a) C11, (b) C40, and (c) C54 structures together with some of the high-symmetry points.

Table 5. The relations between the parameters (a', b', c', β) describing the centred monoclinic unit cell and those of the smaller unit cells of table 1.

Structure	a'	b'	c'	β
C11	c	$\sqrt{2}a$	$3\sqrt{2}a$	90°
C40	$\sqrt{3}a$	a	$2c$	90°
C54	a	b	$(1/2)\sqrt{9c^2 + a^2}$	$90^\circ + \tan^{-1}(a/3c)$

by $\boldsymbol{a}'$, $\boldsymbol{b}'$, and $\boldsymbol{c}$, while those of the smaller unit cells are left unprimed, the definition of the monoclinic unit cell is as given in table 5. We stress that the basis vectors of table 1 may not be parallel to those of table 5.

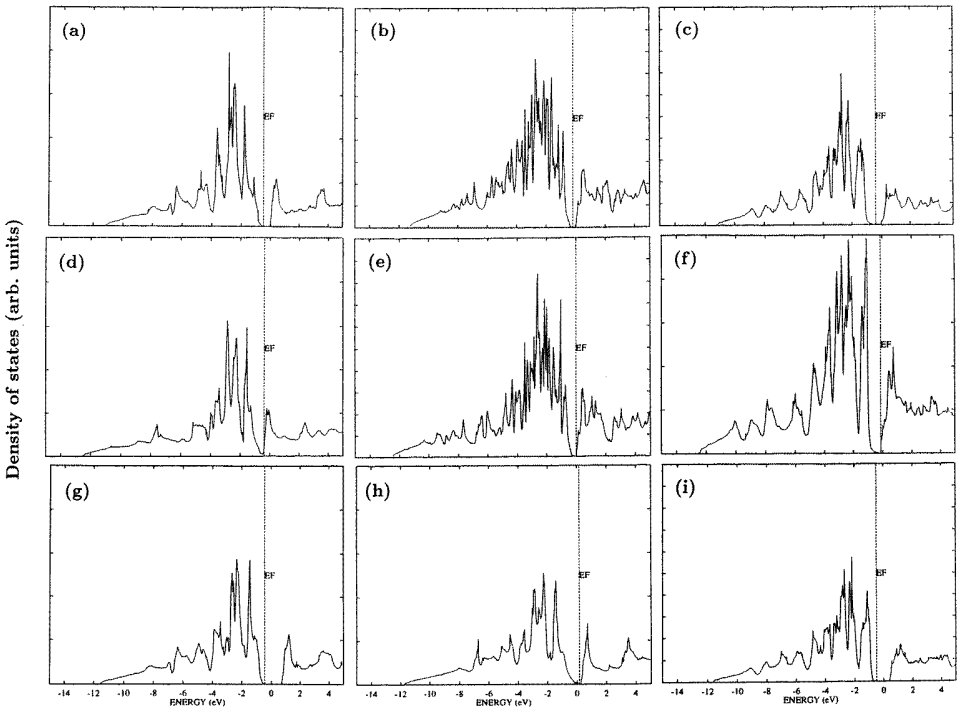

Figure 3. The total density of states per unit cell of (a)–(c) $RuAl_2$, (d)–(f) $RuGa_2$, and (g)–(i) $OsAl_2$ in ((a), (d), (g)) the C11, ((b), (e), (h)) the C40, and ((c), (f), (i)) the C54 crystal structures. The vertical dashed lines indicate the Fermi level. Each unit cell contains one, three, and two formula units for the C11, C40, and C54 structures, respectively.

3. Results

As indicated in table 3, we optimized only one structure, i.e. that of $OsAl_2$ in the C11 crystal structure. On comparing the results with the experimental structure (cf. table 3) we see that there is a very good agreement. This is a far from trivial result, first of all due to the atomic-sphere approximation (the ASA; cf. section 2). Within this approximation one may intuitively expect that symmetry-lowering distortions or structural changes whose total-energy changes are largely dictated by non-spherical parts of the potential will be only poorly described. But obviously this is not the case for the present compounds, which thus shows that the approximations applied are justified. On the other hand, the total-energy lowering for $OsAl_2$ in the C11 structure due to the structure optimization is very small (only about 15 meV per formula unit), which suggests that the system is soft.

For all three compounds we found that the C54 structure had the lowest total energy, with that of the C40 structure only slightly higher (less than 0.1 eV per formula unit). On the other hand, the C11 structure clearly had the highest total energy (between 0.3 and 0.6 eV per formula unit higher). These results were found using the common monoclinic unit cell described in table 5, and since for $OsAl_2$ they are in conflict with the experimental observation, we conclude that the relative stability of the different structures is not described sufficiently accurately within the ASA.

The band structures and the densities of states, in particular around the Fermi level,

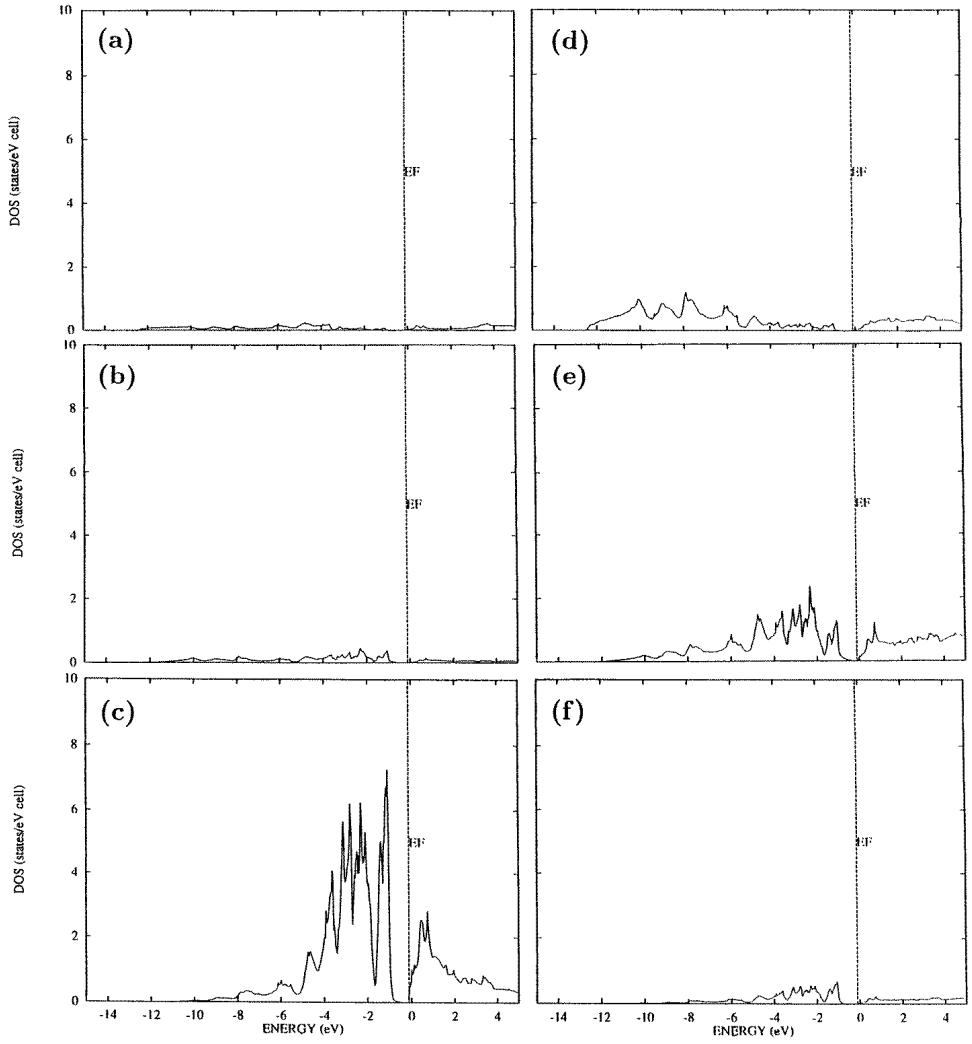

Figure 4. The density of states of $RuGa_2$ in the C54 structure (figure 3(f)) decomposed into contributions from (a) s, (b) p, and (c) d functions on Ru, and (d) s, (e) p, and (f) d functions on Ga.

account for the qualitative aspects of the optical properties. Therefore, we shall now discuss these.

In figure 3 we show the total density of states per unit cell for the three compounds and three crystal structures. It is immediately seen that all of the curves are very similar. The systems are found to be either purely semiconducting with, however, a relatively small gap around the Fermi level, or at least to have a very small density of states at ϵ_F. Moreover, the density of states rises more steeply on the unoccupied side of ϵ_F than on the occupied side, which, as we shall see below, is due to some very flat bands just above ϵ_F. The similarity of nearest and next-nearest neighbours, and the chemical similarities of the constituents explain the similarities of the panels in figure 3.

Also, the total valence-band widths are very similar for all of the systems: they are

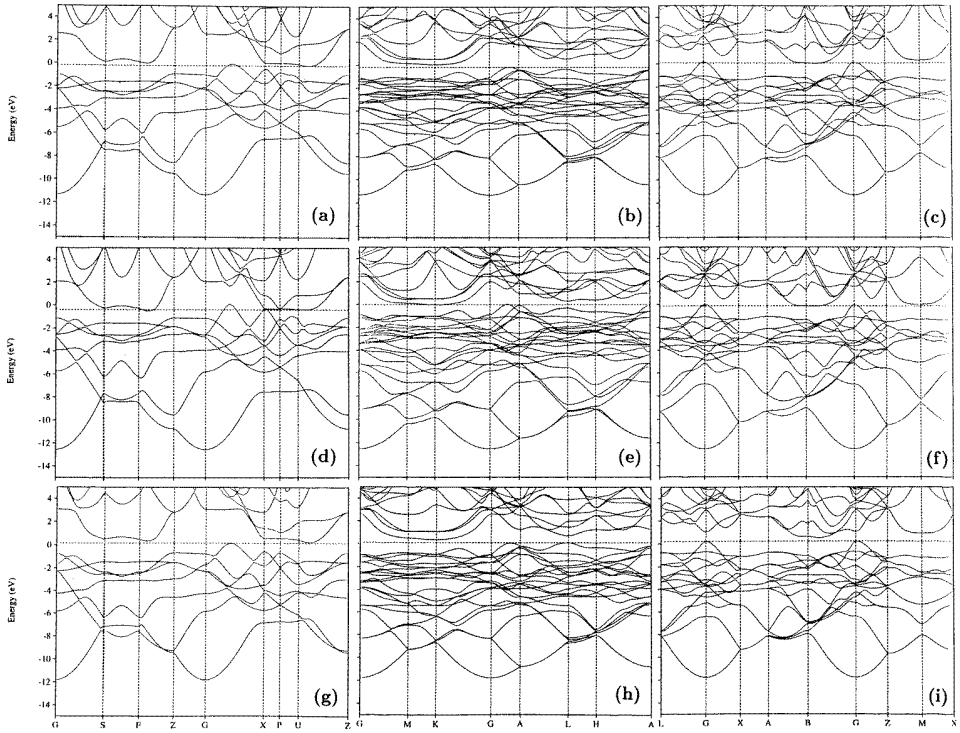

Figure 5. The band structures along some high-symmetry lines (cf. figure 2) for the same compounds and structures as in figure 3. 'G' is the Γ point, 'S' is the Σ point, and the horizontal dashed lines mark the Fermi level.

around 12 eV for $RuGa_2$ and $OsAl_2$, but only about 11 eV for $RuAl_2$. The largest differences are as regards the size of the gap, where there are some variations for the different compounds and/or structures. In all cases, however, the difference is less than 1 eV, and although the density-functional calculations with a local-density approximation tend to underestimate its size, it is clear that these materials are to be considered small-gap semiconductors (see also the band structures to be discussed below). However, $OsAl_2$ appears to have a slightly larger gap, and since a larger electron transfer between M and X is found here (see below) this suggests that the size of the gap can be influenced by electron transfer.

Due to the similarity of all of the results in figure 3, we show in figure 4 the atom- and *l*-decomposed density of states for just one system, i.e. $RuGa_2$ in the C54 structure. From this it is clear that the states around the Fermi level are mainly due to d functions on the transition-metal atoms with some contributions from p functions on Ga (or Al), and that s functions on Ga (or Al) contribute to the lower parts of the occupied parts of the densities of states.

Our results agree well with those found previously for $RuAl_2$ [3, 5] and $RuGa_2$ [3] in the C54 structure. The results of Nguyen Manh *et al* [3] also showed that the occurrence of a (pseudo-) gap at ϵ_F was not due to a charge transfer between the two types of atom, but rather to a hybridization between d functions on the transition-metal atoms and s and p functions on Al or Ga. Due to the similarity between our results and theirs, we have no reason to doubt this conclusion, although the results for $OsAl_2$ suggest that further effects

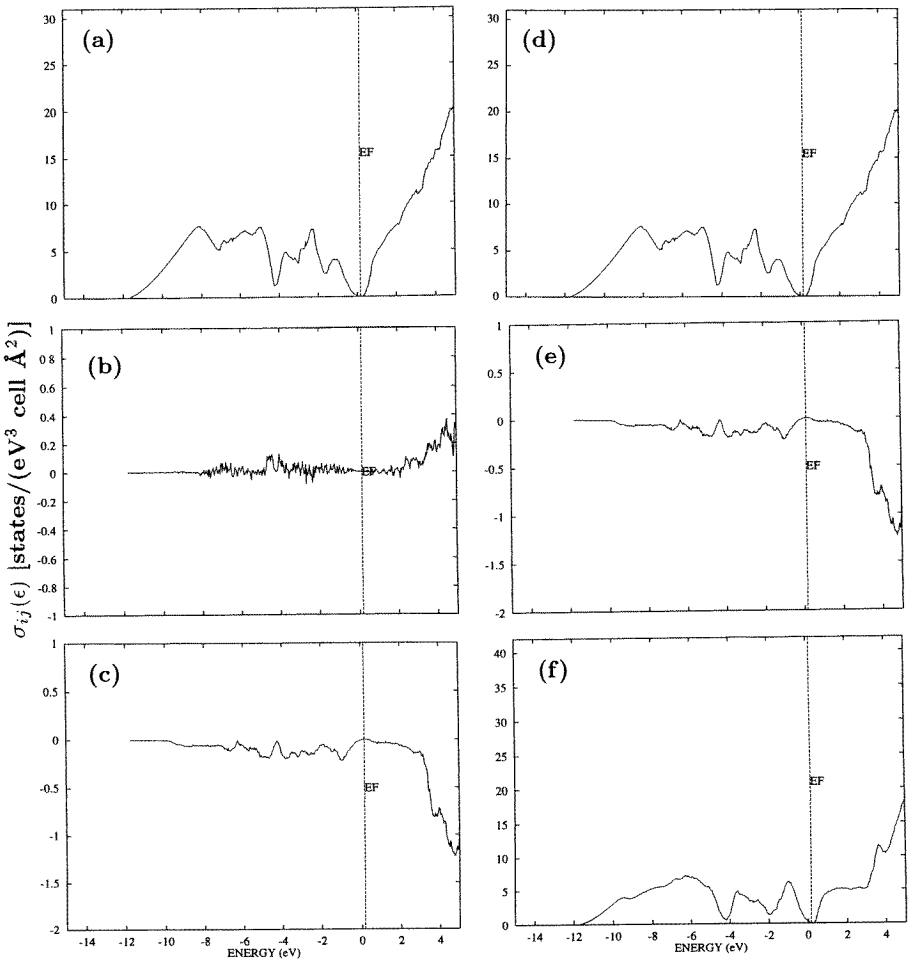

Figure 6. $\tilde{\sigma}_{ij}$ for the C11 structure of $OsAl_2$. (i, j) equals (x, x), (x, y), (x, z), (y, y), (y, z), and (z, z) for the six panels (a), (b), (c), (d), (e), and (f), respectively. z is parallel to the Al–Os–Al units of figure 1(c), and the other two directions are equivalent.

due to electron transfers can appear. Counting the number of electrons inside the various spheres gives the result that at most ± 0.1 electrons per transition-metal atom are transferred to the Al or Ga atoms for the Ru-based compounds. These numbers could have different signs for different structures, and we consider them to be so small that they are essentially vanishing. However, for $OsAl_2$ there was a clearer tendency for the calculations to predict 0.2 electrons to be transferred to the Al atoms from each Os atom.

Equivalently to the results of figure 3, we show in figure 5 the band structures along some of the high-symmetry lines in the first Brillouin zone (see figure 2). For all of the systems the uppermost valence band has a larger curvature than the lowest conduction band. This indicates a higher mobility for p-doped materials than for n-doped ones. The band structures also clearly show that the gaps at the Fermi level are small if not even vanishing (note, however, that due to the standard underestimation of band gaps with local-density calculations, the true gaps are most probably non-zero).

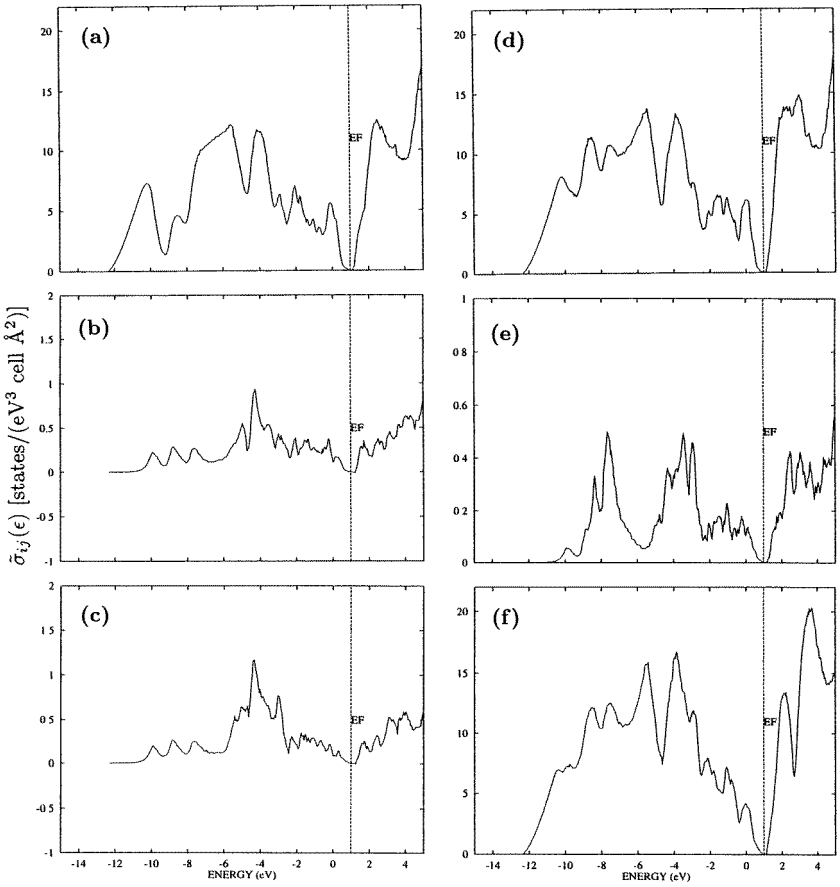

Figure 7. As figure 6, but for the C54 structure of $RuGa_2$. In this case, however, the x-axis is parallel to the Ga–Ru–Ga units of figure 1(f), and the z-axis is perpendicular to the plane of figure 1(f).

For the sake of completeness we add that our band structures are very similar to those obtained previously for $RuGa_2$ [3] and for $RuAl_2$ [5, 9]. As mentioned above, the earlier studies did not consider any structure except the C54 one.

As described in the previous section, the transport properties are here analysed through the quantity $\tilde{\boldsymbol{\sigma}}$. In figure 6 we show this for the C11 structure for $OsAl_2$, i.e. for the system for which figure 3(g) shows the density of states and figure 5(g) the band structures. Equivalently, figure 7 shows $\tilde{\boldsymbol{\sigma}}$ for the C54 structure of $RuGa_2$. Since these systems are semiconducting according to our calculations, we do not need to worry about whether a non-vanishing density of states at the Fermi level is an artifact of the local-density approximation or a real feature, and, thus, about the details concerning the region nearest to the Fermi level.

As discussed in the preceding section, $\tilde{\sigma}_{ij}(\epsilon)$ may vanish for $i \neq j$. For the C11 structure this should be the case, and, furthermore, we shall also have that $\tilde{\sigma}_{xx}(\epsilon) = \tilde{\sigma}_{yy}(\epsilon)$. In figure 6 the latter is clearly seen to be fulfilled, and when the different ordinate scales are taken into account the former is also reasonably well satisfied. By varying the number of points in the $\boldsymbol{k}$-space sampling we found that $\tilde{\sigma}_{ij}(\epsilon)$ was much more sensitive to this number

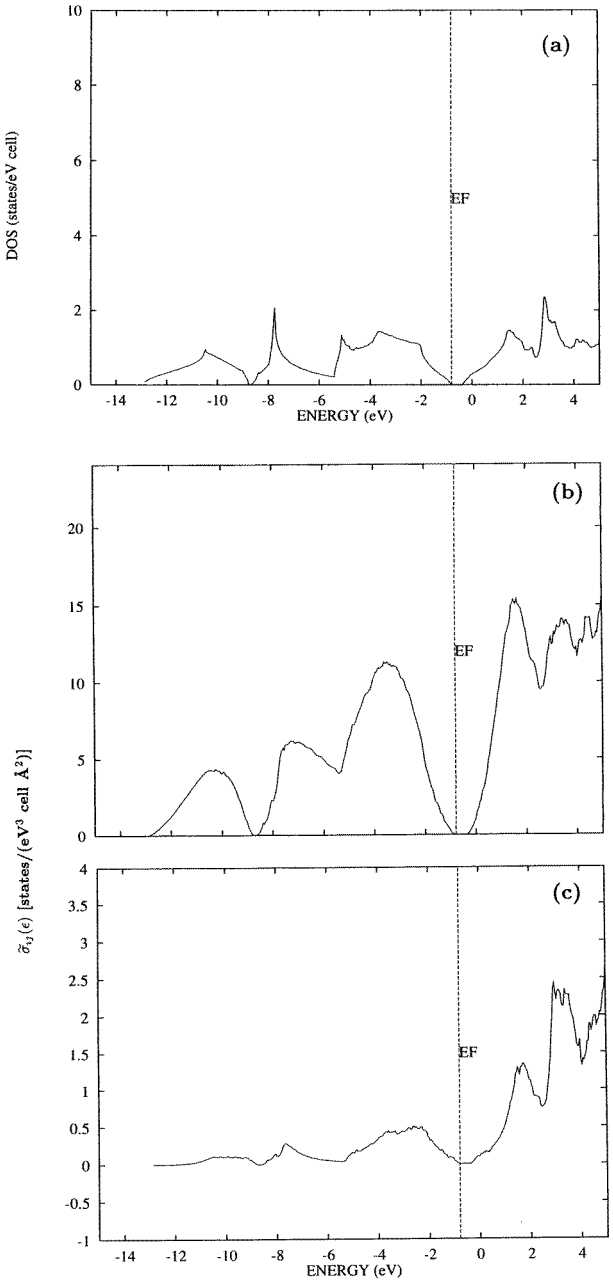

Figure 8. (a) The density of states, (b) one of the diagonal components of $\tilde{\boldsymbol{\sigma}}$, and (c) one of the off-diagonal components of $\tilde{\boldsymbol{\sigma}}$ for crystalline Si with two silicon atoms per unit cell.

than, e.g., the densities of states. In particular in energy regions with flat but crossing bands the problems mentioned in section 3 may occur. Thus, the deviations from exact cancellation of the off-diagonal elements of $\tilde{\sigma}_{ij}(\epsilon)$ are due to the discretization of $\boldsymbol{k}$-space. However, as equations (4)–(6) show, only those parts of $\tilde{\boldsymbol{\sigma}}(\epsilon)$ for energies ϵ that are within roughly kT

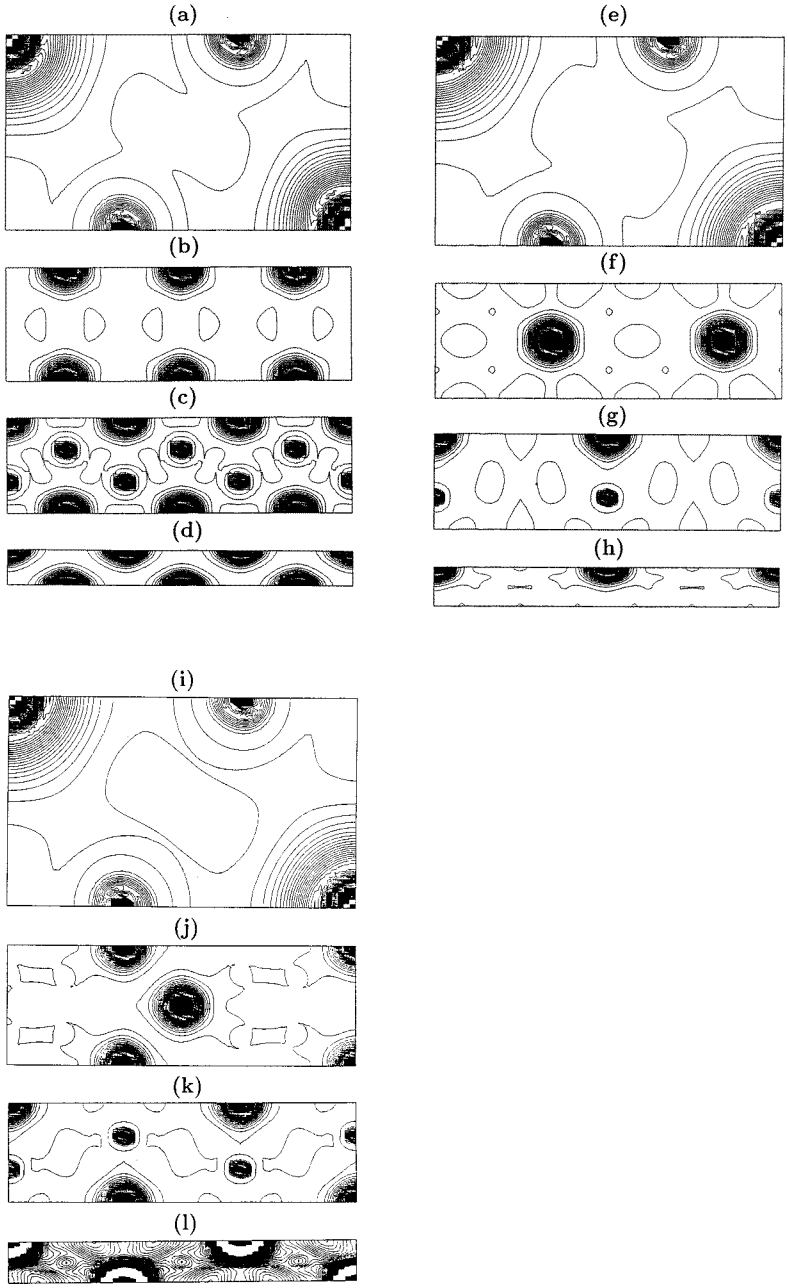

Figure 9. Contour plots of the total valence-electron density for $RuGa_2$ for (a)–(d) the C11 structure, (e)–(h) the C40 structure, and (i)–(l) the C54 structure. The lowest left-hand corner of each panel corresponds to the origin of the coordinate systems (cf. figure 1). The planes are those spanned by ((a), (e), (i)) $\boldsymbol{a}'$ and $\boldsymbol{b}'$, ((b), (f), (j)) $\boldsymbol{c}'$ and $\boldsymbol{a}'+\boldsymbol{b}'$, ((c), (g), (k)) $\boldsymbol{c}'$ and $\boldsymbol{a}'$, and ((d), (h), (l)) $\boldsymbol{c}'$ and $\boldsymbol{b}'$. 60 equally spaced contour values between 0 and 1 au have been chosen. The larger 'atoms' correspond to Ru and the smaller ones to Ga.

of ϵ_F will contribute to the transport properties, and therefore only the parts closest to the gap are relevant for doped materials also. Comparing the $\tilde{\sigma}_{xx}$-, $\tilde{\sigma}_{yy}$-, and $\tilde{\sigma}_{zz}$-components we see that they are very similar close to the Fermi level with, however, a slightly steeper rise above ϵ_F than below it. Although here the flatter bands (cf. figure 5(g)) make the velocities smaller (equation (3)), the larger density of states (figure 3(g)) compensates this. Thus, the large density of states and small band gap should make these systems interesting semiconductors from a transport-property point of view. Since all of the systems studied here have very similar band structures and densities of states, we believe this conclusion to be generally valid for all of the systems considered in this work.

For the C54 structure also, the off-diagonal components of $\tilde{\sigma}$ should vanish, but as seen in figure 7 this is not exactly fulfilled, although the errors, especially around the Fermi level, are small. Furthermore, the different diagonal components are now not forced to be identical due to symmetry restrictions, although they share many features. Comparing figures 6 and 7 and taking into account the fact that the C11 structure has only one formula unit per unit cell, whereas the C54 structure has two formula units per unit cell, we see that the two materials have very similar transport properties. However, the asymmetry about the Fermi level is more pronounced in figure 7 than in figure 6.

In order to arrive at a more quantitative estimate of the transport properties of the present compounds we compare the results with similar ones obtained for crystalline Si. Thus, in figure 8 we show the density of states as well as one of the diagonal components and one of the off-diagonal components of $\tilde{\boldsymbol{\sigma}}(\epsilon)$. We see that the present systems compare well with Si, even when taking into account the fact that the unit cell of Si only contains two atoms. Thus, assuming a rigid-band model to be valid, the materials of the present work should, when doped, have transport properties comparable to those of silicon. When in addition one takes into account the fact that the present compounds have different (i.e. smaller) band gaps, they should be interesting from a technological point of view.

Finally, figure 9 shows contour maps of the valence-electron density for the three different structures for $RuGa_2$. Those of the other compounds are very similar, and are therefore not shown here. The densities in the planes of figure 1 (i.e. figures 9(a), 9(e), and 9(i)) demonstrate the similarity of the different structures, whereas the other densities reflect the different stackings of the planes of figure 1.

4. Conclusions

In the present work we have reported the results of first-principles calculations on three intermetallic semiconductors, each in three different crystal structures. As demonstrated in figure 1, these structures are closely interrelated, and it turned out that the electronic properties varied only little for the different structures. This indicates in turn that their properties are mainly dictated by nearest-neighbour interactions.

The band structures for all of the compounds and structures are very similar. Thus, the conclusion reached by Nguyen Manh *et al* [3] for one of the systems that the occurrence of a band gap is due to hybridization remains valid for all of the systems considered here. However, the fact that the gap for the $OsAl_2$ compounds is larger than those of the other compounds and that there is a larger electron transfer for this material indicates that charge transfers and electrostatics can also influence the size of the gap.

First-principles calculations of transport properties are much less common than those of the optical properties. In the present work we have proposed a parameter-free method for studying the current densities based on analysing the integrand of the current-density matrices. We presented subsequently results for two of the systems. We showed that,

except for minor exceptions, the symmetry constraints that these should obey were largely satisfied, although they were not automatically fulfilled. By comparing with similar results for crystalline silicon we were also able to demonstrate that the present compounds should have transport properties similar to those of silicon, with the additional feature that the band gap is smaller. Due to the density of states being larger above ϵ_F than below it, but despite the smaller carrier velocities, n-doped materials are predicted to have higher thermal and electrical conductivities than p-doped ones.

Acknowledgments

We are very grateful to Ove Jepsen, of the Max-Planck-Institut für Festkörperforschung, Stuttgart, who provided us with most of the computer codes and helped in installing them. The present work was generously supported by the Zentrum für Energieforschung at the University of Konstanz and by the Fonds der Chemischen Industrie.

References

[1] Schwomma O, Nowotny H and Wittmann A 1963 *Monatsh. Chem.* **94** 924
[2] Chaudhury Z A, Sastry G V S and Suryanarayana C 1982 *Z. Metallk.* **73** 201
[3] Nguyen Manh D, Trambly de Laissardière G, Julien J P, Mayou D and Cyrot-Lackmann F 1992 *Solid State Commun.* **82** 329
[4] Pierce F S, Poon S J and Biggs B D 1993 *Phys. Rev. Lett.* **70** 3919
[5] Burkov S E and Rashkeev S N 1994 *Solid State Commun.* **92** 525
[6] Basov D N, Pierce F S, Volkov P, Poon S J and Timusk T 1994 *Phys. Rev. Lett.* **73** 1865
[7] Volkov P and Poon S J 1994 *Europhys. Lett.* **28** 271
[8] Hill E A, Volkov P, Poon S J and Wu Y 1995 *Phys. Rev.* B **51** 4865
[9] Öğüt S and Rabe K M 1996 *Phys. Rev.* B **54** R8297
[10] Edshammar L-E 1965 *Acta Chem. Scand.* **19** 871
[11] Evers J, Oehlinger G and Meyer H 1984 *Mater. Res. Bull.* **19** 1177
[12] Goodman C H L 1985 *Mater. Res. Bull.* **20** 237
[13] Laves F and Wallbaum H J 1939 *Z. Kristallogr.* **101** 78
[14] Jeitschko W 1977 *Acta Crystallogr.* B **33** 2347
[15] Jeitschko W, Holleck H, Nowotny H and Benesovsky F 1963 *Monatsh. Chem.* **94** 838
[16] Nowotny H, Kieffer R and Schachner H 1952 *Monatsh. Chem.* **83** 1243
[17] Nowotny H, Schroth H, Kieffer R and Benesovsky F 1953 *Monatsh. Chem.* **84** 579
[18] Kusma J B and Nowotny H 1964 *Monatsh. Chem.* **95** 1266
[19] Andersen O K 1975 *Phys. Rev.* B **12** 3060
[20] Hohenberg P and Kohn W 1964 *Phys. Rev.* B **133** 864
[21] Kohn W and Sham L J 1965 *Phys. Rev.* **140** A1133
[22] Jepsen O and Andersen O K 1971 *Solid State Commun.* **9** 1763
[23] Lehmann G and Taut M 1972 *Phys. Status Solidi* b **54** 469
[24] Whitlow L W and Hirano T 1995 *AIP. Conf. Proc.* **316** 17
[25] Pauling L 1960 *The Nature of the Chemical Bond* (Ithaca, NY: Cornell University Press)